Developing Diagnostic Tools for Low-Burnup Reactor Samples

Patrick Jaffke,[1,*] Benjamin Byerly,[1,2] Jamie Doyle,[1] Anna Hayes,[1] Gerard Jungman,[1] Steven Myers,[1] Angela Olson,[1] Donivan Porterfield,[1] and Lav Tandon[1]

[1]*Los Alamos National Laboratory, Los Alamos, New Mexico 87545, USA*

[2]*Department of Geology and Geophysics, Louisiana State University, Baton Rouge, Louisiana 70803, USA*

(Received 30 May 2017; revised manuscript received 20 September 2017; published 31 October 2017)

We test common neutron fluence diagnostics in the very-low-burnup regime for natural uranium reactor samples. The fluence diagnostics considered are the uranium isotopics ratios $^{235}U/^{238}U$ and $^{236}U/^{235}U$, for which we find that simple analytic formulas agree well with full reactor simulation predictions. Both ratios agree reasonably well with one another for fluences in the $(\text{mid-}10^{19})\text{-n/cm}^2$ range. However, below about 10^{19} n/cm^2, the concentrations of ^{236}U are found to be sufficiently low that the measured $^{236}U/^{235}U$ ratios become unreliable. We also derive and test diagnostics to determine the cooling times in situations where very low burnup and very long cooling times render many standard diagnostics impractical, such as the $^{241}Am/^{241}Pu$ ratio. We find that using several fragment ratios is necessary to detect the presence of systematic errors such as fractionation.

DOI: 10.1103/PhysRevApplied.8.044025

I. ISOTOPICS INTRODUCTION

Determining the reactor environment that a particular spent fuel sample experienced is critical information for nonproliferation and reactor verification. In particular, the neutron fluence (or exposure) is often related to the fuel burnup and, hence, the plutonium production and grade [1]. This relation makes the fluence an important parameter for nonproliferation and arms reduction [2]. The fluence of a sample can be inferred in many ways, but it is most commonly derived from isotopic ratios of actinides such as $^{235}U/^{238}U$ or $^{236}U/^{235}U$ [3,4] and various plutonium ratios [5]. Additional methods utilize the ratios of activated isotopes in cladding and moderator material, such as the graphite isotope ratio method [6–8], or of ratios of long-lived fragments such as cesium [5,9,10], europium [9], or neodymium [5]. The cooling time is often determined with ratios utilizing short-lived actinides such as $^{241}Pu/^{241}Am$ [11], but it can also be inferred by (γ) spectroscopy of fragments [12]. The cooling time provides one with an estimate of the sample age, which is also pertinent for forensics and nonproliferation.

One can determine the final activities, abundances, and ratios of nuclides with detailed reactor simulations, provided a burnup history and initial fuel composition. Our goal is to invert this process, where one begins with measured isotopic abundances or ratios and then determines the reactor parameters. In particular, we focus on the neutron fluence Φ defined as the time integral of the neutron flux $\phi(t)$, or $\Phi = \int \phi(t)dt$, and the total cooling time T_c defined as the sum of all nonirradiation time. These two parameters can be derived from so-called linear systems, which have simpler analytical forms, in the low-burnup regime. Nonlinear systems can be used to infer parameters, such as the flux and shutdown history [13]. We use low-burnup archived samples available at the Los Alamos National Laboratory. The chemical analyses to determine the abundances of the actinides and fission fragments for our low-burnup samples can be found in Refs. [14,15]. The declared irradiation times of our samples are 85 h or less with thermal fluxes ranging from 10^{13} to 10^{14} $\text{n/cm}^2/\text{sec}$. In this very-low-burnup regime, new cooling time diagnostics must be developed. They are verified alongside the standard fluence diagnostics. Several cooling time diagnostics are utilized to detect the presence of systematic errors.

This paper is structured as follows. The fluence diagnostics are discussed in Sec. II. Cooling time diagnostics are discussed and derived in Sec. III. The diagnostics are verified with reactor simulations, and theoretical errors are generated in Sec. IV. The diagnostics are then applied to low-burnup reactor samples to determine their fluence, cooling time, and sensitivity to systematic errors in Sec. V. We conclude in Sec. VI.

II. FLUENCE DIAGNOSTICS

The fluence diagnostics considered in this work utilize the uranium isotopic ratios $^{235}U/^{238}U$ and $^{236}U/^{235}U$. Ratios utilizing moderator materials cannot be used, as they require a sample removal from the existing reactor, which may not be feasible and impacts future reactor design and safety. In addition, some commonly used long-lived fragments, such as ^{134}Cs or ^{154}Eu, are not produced in sufficient quantities in these very-low-burnup scenarios and create experimental difficulties. Finally, ^{239}Pu cannot be used, as its accumulation is not precisely linear in fluence at low burnup and, thus, displays a flux dependence. For these

*pjaffke@lanl.gov

 © 2017 American Physical Society

reasons, we focus on the uranium ratios above which are trivially related to the fluence via

$$\epsilon(\Phi,\epsilon_0) = \epsilon_0 e^{-\Phi(\sigma^T_{U235}-\sigma^T_{U238})},$$
$$\rho(\Phi) = \left(\frac{\sigma^c_{U235}}{\sigma^T_{U236}-\sigma^T_{U235}}\right)(1-e^{-\Phi(\sigma^T_{U236}-\sigma^T_{U235})}). \quad (1)$$

Here, ϵ denotes the $^{235}U/^{238}U$ ratio and ρ the $^{236}U/^{235}U$ ratio, where ϵ_0 is the initial fuel ratio. The superscripts on the cross sections σ are for capture (c) or total (T) reactions, and we use a one-group fluence for brevity.

As ϵ depends on the initial ratio ϵ_0, a measurement of Φ via the $^{235}U/^{238}U$ ratio is valid only when the initial enrichment is known. In the case of our low-burnup samples, all indicate natural uranium (NU) as the initial fuel [14]. On the other hand, the determination of Φ from ρ is insensitive to the initial fuel, but it requires a measurement of ^{236}U, which is produced in very low quantities when the burnup is low. A final note is that a measurement of Φ using Eq. (1) will be most sensitive to the thermal fluence, as these cross sections dominate (specifically, ^{235}U thermal fission).

Inverting Eq. (1) produces the fluence diagnostics that we apply to the low-burnup samples,

$$\Phi = \frac{\ln(\epsilon_0/\epsilon)}{\sigma^T_{U235}-\sigma^T_{U238}},$$
$$\Phi = \frac{1}{\sigma^T_{U235}-\sigma^T_{U236}}\ln\left(\frac{\sigma^c_{U235}-\rho(\sigma^T_{U236}-\sigma^T_{U235})}{\sigma^c_{U235}}\right). \quad (2)$$

Measurement of the values of ϵ or ρ is typically accomplished by chemical separation [16–18] followed by (γ) spectroscopy [5], thermal ionization mass spectrometry (TIMS) [14], or inductively coupled plasma mass spectrometry [3,4]. Specifically, the measurement of ^{236}U is made difficult as isobaric interferences arise when small quantities of ^{236}U exist amidst large ^{235}U and ^{238}U quantities. Additionally, the α-decay peak of ^{235}U can interfere in a $^{236}U/^{238}U$ measurement done via α spectrometry [19,20].

III. COOLING TIME DIAGNOSTICS

Cooling time diagnostics must be selected specifically for the context of low-burnup samples. For example, the $^{241}Pu/^{241}Am$ ratio cannot be used, as neither ^{241}Pu nor ^{241}Am are produced in appreciable amounts at low burnups. Similar issues preclude the use of other unstable actinides from NU fuel or ^{134}Cs and ^{154}Eu, both of which are nonlinear nuclides [21] that rely on neutron capture as their primary production channel. This preclusion indicates that common cooling time diagnostics that utilize same-species ratios to avoid fractionation [22], such as the $^{134}Cs/^{137}Cs$ ratio [23], are invalid. In addition, our samples exhibit extremely long cooling times (approximately 20 yr), which we define as the sum of all decay periods including shutdowns, which invalidate the use of some major decay heat tags, such as ^{106}Ru and ^{144}Ce [24] as their half-life is too short. Thus, the cooling time diagnostic requires nuclides that are appreciably produced in low-burnup scenarios have long half-lives and are easy to chemically separate and analyze. These requirements naturally lead one to the so-called "linear" fission fragments described by

(a) The linear fragment N_L has a half-life $t^L_{1/2}$ such that $\lambda_L T_{\rm irr} \ll 1$, with $\lambda_L = \ln(2)/t^L_{1/2}$.
(b) The cumulative fission product yields for N_L, $\vec{Z}_L$ are large: $\vec{Z}_L = [Z^L_{U235}, Z^L_{U238}, Z^L_{Pu239}, Z^L_{Pu241}]$.
(c) The (β) parents of N_L have half-lives such that they are in equilibrium during $T_{\rm irr}$.

These fragments are dubbed linear, as their production is linear in Φ, i.e., the number of fissions. Criterion (a) ensures that the fragment is long-lived relative to the irradiation period of the reactor. In our circumstances, where $T_{\rm irr}$ is very short compared to the suspected cooling time T_c, one should modify the criterion (a) so that N_L does not completely decay during the cooling period [i.e., $\lambda_L(T_{\rm irr}+T_c) \ll 1$]. Criterion (b) demands that the fragment is appreciably produced in fission. Criterion (c) allows one to derive a simple analytical expression for N_L, where the yields of the β parents of N_L are accounted for by utilizing the cumulative fission yields of N_L. For our low-burnup purposes, ^{85}Kr, ^{125}Sb, ^{137}Cs, and ^{155}Eu are linear fragments.

Nuclides in a reactor environment are governed by depletion equations, which form the basis for constructing an interaction matrix between the various nuclides. This structure is utilized by many reactor simulation codes [25,26], which often solve these massive (approximately 2000 species) systems as an eigenvalue problem [27]. In our case, we utilize linear fragments to construct a simple isolated system, which resembles a Bateman equation [28],

$$\frac{dN_L}{dt} = -\tilde{\lambda}_L N_L + \vec{Z}_L \cdot \vec{\mathcal{F}}. \quad (3)$$

The positive (negative) terms denote production (depletion) channels, and we use an effective decay constant $\tilde{\lambda} = \lambda + \phi\sigma^T$. We note that the full depletion equation, which resembles Eq. (1) of Ref. [29], reduces to Eq. (3) after applying $\lambda_i \gg b_{j,i}\lambda_j$ [criterion (c)], noting that $\sigma_{j,i}\phi \ll b_{j,i}\lambda_j$ is satisfied for most fragments except for particular reactions such as $^{135}Xe(n,\gamma)^{136}Xe$, and adding an explicit fission term. Thus, Eq. (3) states that a linear fragment N_L is produced via fission at a rate $\vec{Z}_L \cdot \vec{\mathcal{F}} = \sum_f Z^f_L \mathcal{F}^f$, where f runs over the fissiles and $\mathcal{F}^f$ denotes a particular fissile's fission rate, and is depleted through its decay and neutron capture.

Solving Eq. (3) yields

$$N_L(t) = \left(N_{L0} - \frac{\vec{Z}_L \cdot \vec{\mathcal{F}}}{\tilde{\lambda}_L}\right)e^{-\tilde{\lambda}_L t} + \frac{\vec{Z}_L \cdot \vec{\mathcal{F}}}{\tilde{\lambda}_L}, \quad (4)$$

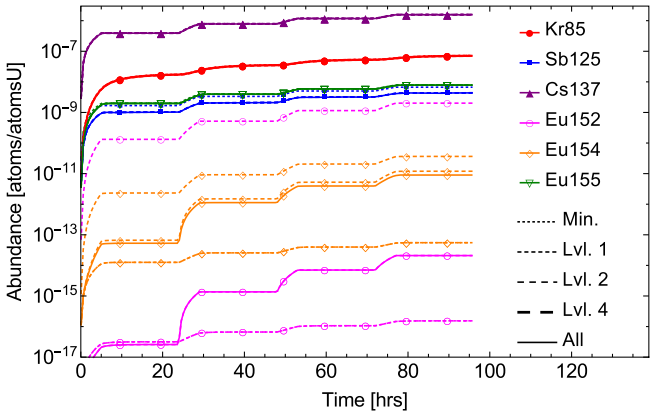

FIG. 1. Relative abundances of several fission fragments from a simulation of an irradiation history consisting of four (5, 19)-h on-off periods and a thermal flux of $\phi_t = 8.5 \times 10^{13}$ n/cm^2/ sec beginning with natural uranium. The simulation uses CINDER08 [30] cross sections, and the decay data are allowed to vary between ENDF7 [31], JEFF [32], and JENDL [33], with no observed difference. Linear fragments show no dependence on the layer of nuclear data.

with an initial nuclide abundance N_{L0}. Most linear fragments satisfy $\lambda_L \gg \phi\sigma_L^T$, but we include the neutron-capture channel in our derivations for completeness. One can easily verify that our selected fragments are linear in nature using reactor simulations. We use a finite-difference method solver for the interaction matrix, where the amount and source of nuclear data can be varied. A sample irradiation history is given by four cycles of (5, 19)-h on-off periods and a thermal flux of $\phi_t = 8.5 \times 10^{13}$n/cm^2/sec. The resulting relative abundances for our linear fragments and for comparison, two nonlinear fragments (^{152,154}Eu), are shown in Fig. 1.

The minimum layer of nuclear data considers just our fragment of interest (FOI). This physically represents the case when each FOI is given by Eq. (4). Layer 1 adds the β parents and their fission yields. Layer 2 adds the production via (n,γ) reactions and their yields. Layer 4 includes the primary, secondary, and (in some cases) tertiary (n,γ) channels as well as all of their β parents with half-lives greater than 30 sec and yields. We also include a simulation of all nuclides with available data (approximately 700). From Fig. 1, one can verify that ^{85}Kr, ^{125}Sb, ^{137}Cs, and ^{155}Eu are linear, as they have very little dependence on the layer of nuclear data. Thus, the linear fragments can be analytically calculated via Eq. (4) using their half-lives and cumulative fission yields instead of solving for each β parent and using their half-life and direct fission yields. None of the fragments studied vary significantly between the major fission yields libraries [31–33].

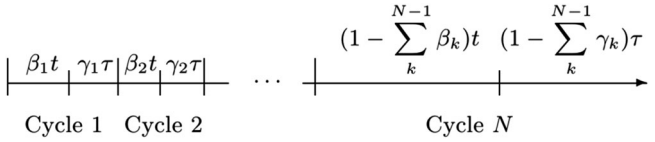

FIG. 2. Generalized irradiation history with N cycles, each consisting of an irradiation time of length $\beta_i t$ and cooling time $\gamma_i \tau$ with multiplicative factors β_i and γ_i that sum to unity. The Nth cycle is the remainder of the total irradiation time t and cooling time τ with time ascending from left to right.

To derive the cooling time diagnostic, we first expand Eq. (4) with $\tilde{\lambda} T_{\rm irr} \ll 1$ [criterion (a)] and arrive at

$$N_L(t, T_c) = \Phi(\vec{Z}_L \cdot \vec{\Sigma}_{\rm fiss}) e^{-\lambda_L T_c} + \mathcal{O}((\tilde{\lambda}_L T_{\rm irr})^2). \quad (5)$$

Equation (5) assumes that $N_{L0} = 0$ and uses the relations $\Phi = \phi t$ and $\vec{\mathcal{F}} = \vec{\Sigma}_{\rm fiss}\phi$. As $\vec{\Sigma}_{\rm fiss}$ is the fission cross sections weighted by the fissile abundances, one can determine $\vec{\Sigma}_{\rm fiss}$ with similar chemical analyses as those used for the fragments [14]. We also account for the decay of N_L after irradiation with the $e^{-\lambda_L T_c}$ term. The expansion to arrive at Eq. (5) is easily valid for all fragments used here, except ^{155}Eu which deviates from it by approximately 1%–3% due to its large cross section.

Universally setting $N_{L0} = 0$ appears to exclude cases with multiple irradiation cycles. Suppose we have a distribution of irradiation and cooling times described in Fig. 2, where t and τ are the total irradiation and cooling times across all cycles. We recursively insert Eq. (4) into itself as an initial condition for the following irradiation and cooling period to verify that distributing the total irradiation and cooling time in a generalized way has a negligible effect on our linear fragments. We find that the final activity ($\alpha_L = \lambda_L N_L$) of a purely linear fragment (i.e., $\tilde{\lambda}_L = \lambda_L$) with a generic distribution of t and τ over N cycles is given by

$$\alpha_L(t, \tau, \vec{\beta}, \vec{\gamma}, N_{L0}) = (\lambda_L N_{L0} - \vec{Z}_L \cdot \vec{\mathcal{F}}) e^{-\lambda_L (t+\tau)} + (\vec{Z}_L \cdot \vec{\mathcal{F}}) e^{-\lambda_L \tau} \times f(\vec{\beta}, \vec{\gamma}), \quad (6)$$

with a preirradiation initial abundance N_{L0}, and the function $f(\vec{\beta}, \vec{\gamma})$ is given as a sum and product of exponentials over the additional $N - 1$ cycles

$$f(\vec{\beta}, \vec{\gamma}) = \left(\prod_{i=1}^{N-1} e^{\lambda_L \gamma_i \tau}\right) + e^{-\lambda_L t} \sum_{i=1}^{N-1} \left[\left(\prod_{j=1}^{i} e^{\lambda_L \beta_j t}\right)\left(\prod_{k=1}^{i-1} e^{\lambda_L \gamma_k \tau}\right) - \left(\prod_{j=1}^{i} e^{\lambda_L (\beta_j t + \gamma_j \tau)}\right)\right]. \quad (7)$$

This complex function for N cycles reduces to unity when $N = 1$. One can show that criterion (a), and the fact that each β_i and γ_i are less than 1 by definition, restricts Eq. (7) to very small deviations from 1. We analyze generic values for the β_i and γ_i within our expected t and τ ranges and find that Eq. (7) is well constrained to $\lesssim$1% deviations from unity. An exception to this is ^{125}Sb, which shows larger deviations when the decay time is concentrated towards earlier cycles (i.e., when $\gamma_1 \gg \gamma_{i\neq 1}$), but this is disfavored for our samples. Thus, with $f(\vec{\beta},\vec{\gamma}) \approx 1$, for any reasonable choice of $\vec{\beta}$ and $\vec{\gamma}$, a single irradiation period of $T_{\rm irr}$ followed by a single cooling time of T_c is equivalent to the case of a series of on-off cycles with total irradiation time $T_{\rm irr}$ and total cooling time, including intermediate shutdowns, T_c.

Now that we have justified our assumption of $N_{L0} = 0$, the final abundance of a linear fragment can be expressed as in Eq. (5). A ratio of the activities of two linear fragments removes the explicit dependence on Φ and creates the expression

$$\alpha_{n,d}(\vec{\Sigma}_{\rm fiss}, T_c) = \frac{\lambda_n \vec{Z}_n \cdot \vec{\Sigma}_{\rm fiss}}{\lambda_d \vec{Z}_d \cdot \vec{\Sigma}_{\rm fiss}} e^{-(\lambda_n - \lambda_d)T_c}, \tag{8}$$

which is a direct measure of the total cooling time. One can correct Eq. (8) with higher-order terms to account for linear fragments with large neutron-capture components, but this will create a dependence on ϕ. For large fast fluences, one must replace $\vec{Z}_i \cdot \vec{\Sigma}_{\rm fiss} \rightarrow \sum_g \Phi_g \times (\vec{Z}_i^g \cdot \vec{\Sigma}_{\rm fiss}^g)$ to account for the different yields in fast fissions.

As mentioned previously, the final value of $\vec{\Sigma}_{\rm fiss}$ is known from a measurement of fissile isotopics. However, $\vec{\Sigma}_{\rm fiss}$ varies over the irradiation period. Therefore, one must average the weighted fission cross sections so as not to bias Eq. (8) towards U or Pu fissions. The averaging is conducted linearly over the fluence Φ because neither $T_{\rm irr}$ nor ϕ are known. One can use the thermal fluence derived from Eq. (2) as the fluence end point, and the initial value of $\vec{\Sigma}_{\rm fiss}$ reflects natural uranium for our samples [14]. This fluence-averaged value $\langle \vec{\Sigma}_{\rm fiss} \rangle_\Phi$ becomes a critical factor when predicting fragments that have cumulative yields that depend strongly on the fissioning nuclide.

Inverting Eq. (8) reveals the cooling time diagnostic

$$T_c = \frac{1}{\lambda_d - \lambda_n} \ln\left(\frac{\alpha_{n,d} \lambda_d \vec{Z}_d \cdot \langle \vec{\Sigma}_{\rm fiss} \rangle_\Phi}{\lambda_n \vec{Z}_n \cdot \langle \vec{\Sigma}_{\rm fiss} \rangle_\Phi} \right). \tag{9}$$

Because of the pole in Eq. (9), two linear fragments with similar decay constants $\lambda_n \simeq \lambda_d$, such as a ratio of ^{90}Sr and ^{137}Cs, can produce large errors in the cooling time, but one can remove these numerically [34]. For fragments with large cross sections, one can expand Eq. (4) to $\mathcal{O}((\tilde{\lambda} T_{\rm irr})^2)$, but this introduces an unverifiable value for $T_{\rm irr}$ and corrects only the cooling time by a few percent.

IV. VERIFICATION

In Secs. II and III, we list the diagnostics for the thermal fluence and cooling time. These diagnostics are verified with the use of the reactor simulation described in Sec. III. Over 70 sample cases are evaluated with layer-4 nuclear data to determine the validity of the analytical calculations. The cases span a range of reasonable values for the thermal flux ϕ_t, cooling time T_c, fast flux ϕ_f, irradiation time $T_{\rm irr}$, number of shutdowns N_s, and shutdown length T_s. The derived values for Φ and T_c, using Eqs. (2) and (9) are compared with those used as input to the simulation. We find that the only parameter that affects the fluence diagnostic is the introduction of a fast flux ϕ_f, as it slightly increases the final ρ and ϵ values, which can be mistaken for a larger thermal fluence. Using the maximum expected fast flux, the diagnostic of Eq. (2) returns the input fluence within approximately 0.5% for both the ^{235}U/^{238}U and ^{236}U/^{235}U ratios. The situation for the cooling time diagnostic is much more complicated.

We use the following ratios for the cooling time diagnostic: ^{137}Cs/^{155}Eu (α_1), ^{137}Cs/^{125}Sb (α_2), and ^{155}Eu/^{125}Sb (α_3). Diagnostics using ^{85}Kr are removed, as it may experience volatile leakage. The derived cooling time is found to vary with all major reactor parameters listed above. As the total Φ_t increases, the errors on Eq. (9) increase linearly, but this is mediated somewhat by linearly averaging $\vec{\Sigma}_{\rm fiss}$. The increase of ϕ_f creates an underestimation of T_c proportional to the additional fast cumulative yields of the fragments used in Eq. (9). Increasing the cooling time serves to decrease the errors on all T_c diagnostics as the deviation from end-of-cycle activity ratios becomes more severe for longer T_c. Finally, the shutdown history has a very small impact, in agreement with $f(\vec{\beta},\vec{\gamma}) = 1$ in Sec. III. The maximum errors in percent due to the use of our analytical expressions for the reactor parameters are provided in Table I.

Overall, from Table I, one can see that the diagnostics derived in Eq. (2) for the fluence have extremely small errors, and one can expect the correct fluence within approximately 0.5%. For the cooling time diagnostic in Eq. (9), the errors are more substantial as the fragment systems are more complex. Overall, our diagnostics return the correct cooling time within approximately 4%, 0.6%, and 3.4% for the ^{137}Cs/^{155}Eu, ^{137}Cs/^{125}Sb, and ^{155}Eu/^{125}Sb ratios, respectively. The linear averaging in Sec. III returns the lowest errors, but it ignores the quadratic behavior of ^{239}Pu at low burnup. The errors in Table I can be effectively eliminated when we account for the nonlinear nature of ^{239}Pu at low burnups and calculate Eq. (9) to $\mathcal{O}((\tilde{\lambda} T_{\rm irr})^2)$. We note that these errors are strictly from the analytical expressions and contain no systematic errors, such as fractionation or experimental uncertainties. We also calculate the expected ^{239}Pu abundance using a similar analytical method with errors of approximately 0.25%, but this

TABLE I. Analytical errors for the fluence ($^{235}U/^{238}U$ and $^{236}U/^{235}U$ ratios) and cooling time ($\alpha_1 = {}^{137}Cs/{}^{155}Eu$, $\alpha_2 = {}^{137}Cs/{}^{125}Sb$, and $\alpha_3 = {}^{155}Eu/{}^{125}Sb$ ratios) diagnostics given by Eqs. (2) and (9). Each cell shows the maximum expected error over a particular reactor parameter (the thermal fluence Φ_t, fast flux ϕ_f, cooling time T_c, number of shutdowns N_s, and length of shutdowns T_s) range. The overall error for each diagnostic is the individual errors summed in quadrature, which provides a conservative maximum.

	Φ diagnostics		T_c diagnostics		
	ϵ	ρ	α_1	α_2	α_3
Φ_t	~0%	~0%	3.86%	0.57%	−3.27%
ϕ_f	0.54%	0.24%	−0.47%	−0.19%	−0.14%
T_c	0%	0%	−0.99%	−0.12%	0.89%
N_s	0%	0%	0.10%	0.01%	−0.10%
T_s	0%	0%	−0.17%	−0.16%	−0.14%
Overall	±0.54%	±0.24%	±4.02%	±0.63%	±3.40%

calculation requires knowledge of both ϕ and T_{irr}, so we exclude it from our analysis. The theory errors of Table I are lower than the experimental measurement errors. With these notes in mind, we use these diagnostics to determine the thermal fluence and extract information about systematic errors from three cooling time diagnostics.

V. EXPERIMENTAL APPLICATION

Ten archived samples are analyzed for their U and Pu isotopics, as well as the activities of several fission fragments. The actinides are separated and measured as described in Ref. [14]. In short, U metal or UO_3 samples are dissolved in HNO_3, then loaded and separated on anion-exchange columns to achieve separation of Pu from U. Isotope ratios and isotope dilution measurements are determined by TIMS. Fission fragments are measured by (γ) spectrometry [15]. Samples *H* and *K* are in UO_3 form, while the remainder are uranium metal.

Both fluence diagnostic methods are attempted, but discrepancies are observed between the $^{236/235}U$ and $^{235/238}U$ ratios in very-low-burnup cases, as shown in Fig. 3. The fluences determined in samples *D* through *K* are all nearly self-consistent. Sample *C* reports fluences that deviate more strongly. Samples *A* and *B* were contaminated with ^{236}U memory effects, so their values are not used. The chemical analyses of the remaining samples corrects the ^{236}U issue. Overall, it appears that our method of extracting the thermal fluence via Eq. (2) is accurate and self-consistent for the majority of samples with $\Phi \geq 10^{19}$ n/cm^2. Below this limit, the low concentrations of ^{236}U create experimental difficulties in acquiring the fluence with multiple methods. Thus, one can determine the thermal fluence with two independent diagnostics in samples with appreciable amounts of ^{236}U but must rely solely on the $^{235/238}U$ ratio in extremely low-burnup

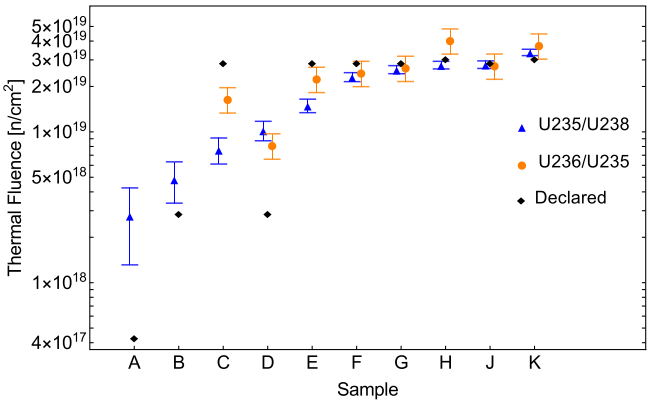

FIG. 3. The derived thermal fluence via the $^{235/238}U$ (triangles) or $^{236/235}U$ (circles) ratios compared with the declared values (diamonds). Both methods are self-consistent and in good agreement with the declared values in higher fluence samples. The $^{236/235}U$ diagnostic cannot be used in samples with trace ^{236}U amounts. Errors are the 1σ experimental and theoretical errors summed in quadrature.

samples with trace levels of ^{236}U. The ϵ diagnostic is valid only when ϵ_0 is known, so the ρ diagnostic should be used if enough ^{236}U is present. The average difference between the two diagnostics is 19.9%.

In determining the total cooling time, we use the ratios identified in Sec. IV. Figure 4 illustrates the agreement and tension between the different diagnostics. A few samples perform relatively well, but most demonstrate disagreement between the three cooling time diagnostics. In particular, the ^{155}Eu-based determinations of T_c show disagreement with the $^{137}Cs/^{125}Sb$ ratio as the inferred fluence rises. Leakage of volatile fission fragments, such as ^{85}Kr, can occur at the $\gtrsim$13% level in PWR fuels [35], so these ratios are removed. A portion of the bias from ^{155}Eu-based diagnostics can be explained by the overestimation of the ^{239}Pu component when linearly averaging $\vec{\Sigma}_{\text{fiss}}$ and the need to compute T_c to second order, but these errors will approach only the 3%–4% level. We note that fission fragments that have very different yields for each fissile, such as ^{155}Eu, will be more dramatically affected by this linear averaging. In our specific case, the natural uranium fuel and very low burnup remove this concern, as the ^{239}Pu fission rate and abundance are orders of magnitude below that of ^{235}U. One can calculate the necessary increase in ^{155}Eu activity to bring all three diagnostics into agreement. These values vary from approximately 10% to about a factor of 3. The samples with higher fluences require larger ^{155}Eu increases, as is expected in the case of fractionation. The average error between the $^{137}Cs/^{125}Sb$ diagnostic and the declared cooling times is 2% for samples *B* through *K*. The ^{125}Sb abundance is not measured in sample *A*. The average diagnostic discrepancy is found to be approximately 37% between the ^{155}Eu-based diagnostics and the

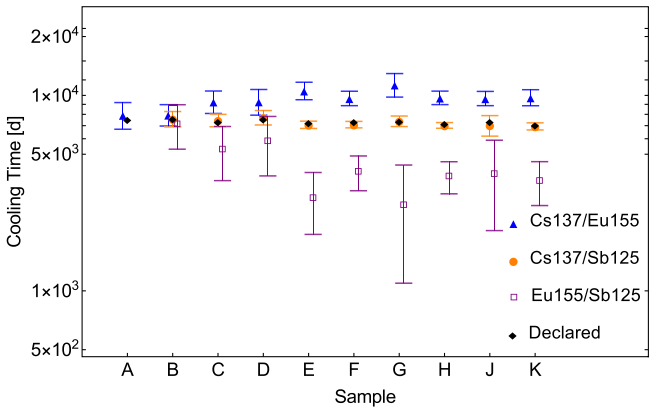

FIG. 4. The derived cooling times via the α_1 (triangles), α_2 (circles), and α_3 (open squares) diagnostics compared with the declared values (diamonds). See text for α definitions. The disagreement between the diagnostics indicates the presence of systematic errors, such as an initial europium abundance or fractionation. Errors are the 1σ experimental and theoretical errors summed in quadrature.

^{137}Cs/^{125}Sb ratio. We note that the use of multiple T_c diagnostics allows one to detect the presence of systematic errors, such as the fractionation of ^{155}Eu, and identify the best nuclides to use as diagnostic tags. This technique must be used in the very-low-burnup regime, as traditional same-species ratios are impractical.

VI. CONCLUSION

The work conducted here demonstrates that the thermal fluence can be determined in low-burnup samples using the ^{235}U/^{238}U and ^{236}U/^{235}U ratios. These ratios are common fluence diagnostics, which we verify with detailed reactor simulations and then experimentally demonstrate to be accurate and self-consistent when enough ^{236}U is produced above the detection threshold. The average discrepancy between the two fluence diagnostics in our low-burnup samples is 19.9% for $\Phi > 10^{19}$ n/cm^2/ sec.

The low burnup of our reactor samples require new cooling time diagnostics to be derived, as the concentrations of standard diagnostic tags are below detection thresholds or long cooling times prohibit their use. The new cooling time diagnostics utilize simple linear fission fragments with long half-lives and considerable fission yields. Four such fragments are identified, and the derived diagnostics are verified in low-burnup scenarios. The experimentally determined cooling times are shown to be consistent in some samples but vary by approximately 37% on average. In addition, leakage of volatile gases invalidates the diagnostics using ^{85}Kr. Overall, the ^{137}Cs/^{125}Sb ratio seems to agree with the sample age across all samples. Differing results for the cooling time, as measured by several diagnostics, can be explained by the fractionation of ^{155}Eu with larger sample fluence, even in the very-low-burnup regime.

The fluence and cooling time derivation should be conducted in tandem, where the Φ determination is used to derive $\langle\vec{\Sigma}_{\rm fiss}\rangle_\Phi$ and verify that the sample has a burnup low enough to validate the simple analytical expressions for T_c. This work provides verification of fluence diagnostics and new cooling time diagnostic techniques to determine the presence of systematic errors in low burnup samples, both of which have applications in nonproliferation and verification.

ACKNOWLEDGMENTS

We would like to thank the analytical chemistry team: L. Colletti, E. Lujan, K. Garduno, T. Hahn, L. Walker, A. Lesiak, P. Martinez, F. Stanley, R. Keller, M. Thomas, K. Spencer, L. Townsend, D. Klundt, D. Decker, and D. Martinez. Los Alamos National Laboratory supports this work through LDRD funding.

[1] A. V. Stepanov, T. P. Makarova, B. A. Bibichev, A. M. Fridkin, A. V. Lovtsyus, L. D. Preobrazhenskaya, A. A. Lipovskii, and A. N. Timofeev, Determination of burnup and isotope composition for spent VVÉR-365 fuel, Sov. J. At. En. **49**, 673 (1980).

[2] Thomas W. Wood, Bruce D. Reid, John L. Smoot, and James L. Fuller, Establishing confident accounting for Russian weapons plutonium, Nonprolif. Rev. **9**, 126 (2002).

[3] Sergei F. Boulyga and J. Sabine Becker, Isotopic analysis of uranium and plutonium using ICP-MS and estimation of burn-up of spent uranium in contaminated environmental samples, J. Anal. At. Spectrom. **17**, 1143 (2002).

[4] Sergei F. Boulyga and Klaus G. Heumann, Determination of extremely low 236U/238U isotope ratios in environmental samples by sector-field inductively coupled plasma mass spectrometry using high-efficiency sample introduction, Journal of Environmental Radioactivity **88**, 1 (2006).

[5] Jung Suk Kim, Young Shin Jeon, Soon Dal Park, Yeong-Keong Ha, and Kyuseok Song, Analysis of high burnup pressurized water reactor fuel using uranium, plutonium, neodymium, and cesium isotope correlations with burnup, Nucl. Eng. Technol. **47**, 924 (2015).

[6] B. D. Reid, W. C. Morgan, E. F. Love, Jr., D. C. Gerlach, S. L. Peterson, J. V. Livingston, L. R. Greenwood, and J. P. McNeece, Pacific Northwest National Lab Report No. PNNL-13056, 1999.

[7] C. J. Gesh, Pacific Northwest National Lab, Report No. PNNL-14568, 2004.

[8] Alex Gasner and Alexander Glaser, Nuclear archaeology for heavy-water-moderated plutonium production reactors, Sci. Global Secur. **19**, 223 (2011).

[9] S. Caruso, M. Murphy, F. Jatuff, and R. Chawla, Validation of 134Cs, 137Cs and 154Eu single ratios as burnup monitors for ultra-high burnup {UO2} fuel, Ann. Nucl. Energy **34**, 28 (2007).

[10] S. A. Ansari, M. Asif, T. Rashid, and K. G. Qasim, Burnup studies of spent fuels of varying types and enrichment, Ann. Nucl. Energy **34**, 641 (2007).

[11] Klaus Mayer, Maria Wallenius, and Zsolt Varga, Nuclear forensic science: Correlating measurable material parameters to the history of nuclear material, Chem. Rev. **113**, 884 (2013).

[12] Ian Gauld and Matthew Francis, Investigation of passive gamma spectroscopy to verify spent nuclear fuel content, in *Proceedings of the 51st Annual Meeting of the Institute of Nuclear Materials Management (INMM)*, 2010, https://inis.iaea.org/search/searchsinglerecord.aspx?recordsFor=SingleRecord&RN=42005537.

[13] A. C. Hayes and Gerard Jungman, Determining reactor flux from xenon-136 and cesium-135 in spent fuel, Nucl. Instrum. Methods Phys. Res., Sect. A **690**, 68 (2012).

[14] Benjamin Byerly, Lav Tandon, Anna Hayes-Sterbenz, Patrick Martinez, Russ Keller, Floyd Stanley, Khalil Spencer, Mariam Thomas, Ning Xu, and Michael Schappert, Determination of initial fuel state and number of reactor shutdowns in archived low-burnup uranium targets, J. Radioanal. Nucl. Chem., DOI: (2015).

[15] Lav Tandon *et al.*, Establishing reactor operations from uranium targets used for the production of plutonium, J. Radioanal. Nucl. Chem. **282**, 573 (2009).

[16] H. Natsume, H. Umezawa, S. Okazaki, T. Suzuki, T. Sonobe, and S. Usuda, Sequential ion-exchange separation of heavy elements and selected fission products for burnup measurement, J. Nucl. Sci. Technol. **9**, 737 (1972).

[17] R. M. Abernathey, G. M. Matlack, and J. E. Rein, Sequential ion exchange separation and mass spectrometric determination of neodymium, uranium, and plutonium in mixed oxide fuels for burnup and isotopic distribution measurements, in *Analytical Methods in the Nuclear Fuel Cycle* (1971), pp. 513–521, http://www.iaea.org/inis/collection/NCLCollectionStore/_Public/03/025/3025619.pdf.

[18] S. F. Marsh, M. R. Ortiz, and R. M. Abernathey, Los Alamos National Lab Report No. LA-5568, 1974.

[19] A. Martín Sánchez, F. Vera Tomé, J. Díaz Bejarano, and M. Jurado Vargas, A rapid method for determination of the isotopic composition of uranium samples by alpha spectrometry, Nucl. Instrum. Methods Phys. Res., Sect. A **313**, 219 (1992).

[20] J. L. Iturbe, Identification of ^{236}U in commercially available uranium compounds by alpha particle spectrometry, Appl. Radiat. Isot. **43**, 817 (1992).

[21] Patrick Huber and Patrick Jaffke, Neutron Capture and the Antineutrino Yield from Nuclear Reactors, Phys. Rev. Lett. **116**, 122503 (2016).

[22] E. C. Freiling and M. A. Kay, Radionuclide fractionation in air-burst debris, Nature (London) **209**, 236 (1966).

[23] J. Navarro, R. Aryaeinejad, and D. W. Nigg, A feasibility study to determine cooling time and burnup of ATR fuel using a nondestructive technique and three types of gamma-ray detectors, in *Reactor Dosimetry: 14th International Symposium*, edited by David Vehar, Douglas Selby, and Mary Sparks (2012), https://www.astm.org/DIGITAL_LIBRARY/STP/SOURCE_PAGES/STP1550.htm.

[24] B. Bergelson, A. Gerasimov, and G. Tikhomirov, Influence of high burnup on the decay heat power of spent fuel at long-term storage, in *Proceedings of the International Conference Nuclear Energy for New Europe* (2005), https://inis.iaea.org/search/search.aspx?orig_q=RN%3A37104778.

[25] Oak Ridge National Laboratory, *Scale: A Comprehensive Modeling and Simulation Suite for Nuclear Safety Analysis and Design*, 6th ed. (Oak Ridge National Laboratory, Oak Ridge, Tennessee, 2011).

[26] O. Meplan, A. Nuttin, O. Laulan, S. David, F. Michel-Sendis, and J. Wilson, MURE : MCNP Utility for Reactor Evolution - Description of the methods, first applications and results, in ENC 2005–European Nuclear Conference. Nuclear Power for the XXIst Century : From Basic Research to High-Tech Industry (2009), http://hal.in2p3.fr/in2p3-00025308/document.

[27] Maria Pusa and Jaakko Leppänen, Computing the matrix exponential in burnup calculations, Nucl. Sci. Eng. **164**, 140 (2010).

[28] H. Bateman, The solution of a system of differential equations occurring in the theory of radioactive transformations, Proc. Cambridge Philos. Soc. **15**, 423 (1910).

[29] A. E. Isotalo and P. A. Aarnio, Comparison of depletion algorithms for large systems of nuclides, Ann. Nucl. Energy **38**, 261 (2011).

[30] S. Holloway and W. B. Wilson, CINDER08: The next generation, in *Proceedings of First International Workshop on Accelerator Radiation Induced Activation (ARIA'08), Villigen, Switzerland* (Paul Scherrer Institute, Villigen, 2009).

[31] M. B. Chadwick *et al.*, ENDF/B-VII.1 nuclear data for science and technology: Cross sections, covariances, fission product yields and decay data, Nucl. Data Sheets **112**, 2887 (2011).

[32] M. A. Kellett, O. Bersillon, and R. W. Mills, *The JEFF-3.1/-3.1.1 Radioactive Decay Data and Fission Yields Sub-Libraries* (Nuclear Energy Agency, 2009).

[33] K. Shibata, O. Iwamoto, T. Nakagawa, N. Iwamoto, A. Ichihara, S. Kunieda, S. Chiba, K. Furutaka, N. Otuka, T. Ohsawa, T. Murata, H. Matsunobu, A. Zukeran, S. Kamada, and J. Katakura, JENDL-4.0: A new library for nuclear science and engineering, J. Nucl. Sci. Technol. **48**, 1 (2011).

[34] Jerzy Cetnar, General solution of Bateman equations for nuclear transmutations, Ann. Nucl. Energy **33**, 640 (2006).

[35] V. Metz *et al.*, Report No. CP-FP7-295722, 2013, http://www.firstnuclides.eu/ZonaPublica/WP1_deliverable_D1_2.pdf.